ACS OMEGA

Article

Cite This: ACS Omega 2020, 5, 1656−1668

Doxorubicin Loading on Functional Graphene as a Promising Nanocarrier Using Ternary Deep Eutectic Solvent Systems

Mohamad Hamdi Zainal-Abidin,[†,‡] Maan Hayyan,[*,‡,∥] Gek Cheng Ngoh,[*,†,⊥] and Won Fen Wong[§]

[†]Department of Chemical Engineering, Faculty of Engineering, [‡]University of Malaya Centre for Ionic Liquids (UMCiL), Faculty of Engineering, [§]Department of Medical Microbiology, Faculty of Medicine, and [⊥]Centre for Separation Science and Technology (CSST), Department of Chemical Engineering, Faculty of Engineering, University of Malaya, Kuala Lumpur 50603, Malaysia

[∥]Chemical Engineering Program, Faculty of Engineering & Technology, Muscat University, PO Box 550, Muscat P.C.130, Sultanate of Oman

ABSTRACT: The application of graphene in the field of drug delivery has attracted massive interest among researchers. However, the high toxicity of graphene has been a drawback for its use in drug delivery. Therefore, to enhance the biocompatibility of graphene, a new route was developed using ternary natural deep eutectic solvents (DESs) as functionalizing agents, which have the capability to incorporate various functional groups and surface modifications. Physicochemical characterization analyses, including field emission scanning electron microscope, fourier-transform infrared spectroscopy, Raman spectroscopy, Brunauer−Emmett−Teller, X-ray diffraction, and energy dispersive X-ray, were used to verify the surface modifications introduced by the functionalization process. Doxorubicin was loaded onto the DES-functionalized graphene. The results exhibited significantly improved drug entrapment efficiency (EE) and drug loading capacity (DLC) compared with pristine graphene and oxidized graphene. Compared with unfunctionalized graphene, functionalization with DES choline chloride (ChCl):sucrose:water (4:1:4) resulted in the highest drug loading capacity (EE of 51.84% and DLC of 25.92%) followed by DES ChCl:glycerol:water (1:2:1) (EE of 51.04% and DLC of 25.52%). Following doxorubicin loading, graphene damaged human breast cancer cell line (MCF-7) through the generation of intracellular reactive oxygen species (>95%) and cell cycle disruption by increase in the cell population at S phase and G2/M phase. Thus, DESs represent promising green functionalizing agents for nanodrug carriers. To the best of our knowledge, this is the first time that DES-functionalized graphene has been used as a nanocarrier for doxorubicin, illustrating the potential application of DESs as functionalizing agents in drug delivery systems.

INTRODUCTION

Doxorubicin (DOX; also known as adriamycin) is an effective antineoplastic chemotherapy drug that is normally applied to treat breast cancer. DOX has been used in the treatment of various other cancers, including acute lymphocytic leukemia, Kaposi's sarcoma, osteogenic sarcomas, bladder cancer, and lymphoma.[1−5] However, there is a need to improve conventional delivery of DOX, which lacks efficiency and selectivity against cancerous cells.[6] Systemic delivery of DOX is highly critical to enhance the therapeutic application of DOX.

Development of noninvasive drug administration approaches is a growing interest in drug delivery studies. In this context, several important issues arise in the field of drug delivery, namely, drug efficacy, selectivity of drugs between cancerous and normal cells, and limited cellular entry of drugs.[7−9] Nanodrug carriers represent an alternative way of increasing the efficiency of drug delivery as well as the pharmaceutical activity of drugs.[10,11] Therefore, currently, the development of novel nanodrug carriers, which is currently known as nanomedicine, is a focal point in modern medicine.

Since its discovery, graphene has been widely explored in various fields, including electronics, engineering, biomedicine, and chemistry.[12−14] Graphene has a two-dimensional (2-D) structure comprised of sp^2 hybridized carbon atoms with delocalized π electrons on their planar aromatic rings.[12,15] Graphene has a large surface area, high biocompatibility, high intrinsic mobility, high Young's modulus (elastic modulus), and high thermal stability. Recently, graphene has been introduced as a potential nanocarrier for drug loading via π-π stacking and hydrophobic and electrostatic interactions.[16] Because of its high surface area, graphene can provide multiple attachment sites for drug targeting. Graphene has higher drug loading capacity (i.e., up to a 200% loading ratio of loaded drug weight to vehicle) compared with other nanodrug carrier systems, such as single-walled carbon nanotubes.[15] Graphene has been used as a nanocarrier for numerous bioactive compounds and drugs, such as ibuprofen, DOX, heparin,

Received: November 2, 2019
Accepted: December 23, 2019
Published: January 15, 2020

DOI: 10.1021/acsomega.9b03709
ACS Omega 2020, 5, 1656−1668

ellagic acid, 5-fluorouracil, and camptothecin.[13,17,18] However, there is speculation that graphene is potentially toxic to humans and the environment.[12] Aggregation or flocculation of graphene on cell membranes is presumed to play a primary role in its cellular toxicity.[19,20] Therefore, it is important to modify the surface chemistry of graphene, which may improve the biocompatibility of graphene with cells and biological macromolecules.

Functionalization is a process that includes the addition of new functional groups to the surface of the nanoparticles through chemical or physical attachment.[21] However, there are some adverse concerns regarding the conventional functionalization agents (e.g., poly(ethylene glycol) and poly lactic-*co*-glycolic acid), such as involving a multistep and complicated procedure, time consumption, requirement of high temperature (above 100 °C), and use of a highly corrosive solution, resulting in high cost of the whole process.[22−26]

Over the past decade, deep eutectic solvents (DESs) have been deemed to be promising green multitasking solvents for replacing hazardous organic solvents in many applications. DES was introduced by Abbott et al.[27] as a eutectic mixture prepared through a complexation of two or more Lewis or Brønsted acids and bases that has a lower melting point than its single components.[28] DESs have been used in numerous chemical and biochemical applications.[28−33] One of these is for their role as promising functionalizing agents for carbon nanomaterials.[34,35] The functionalization using DESs may lead to surface modifications and introduce new functional groups, which result in significant enhancement in the dispersion stability of the aqueous solutions containing carbon nanomaterials. The improved biocompatibility of graphene has been witnessed by the interaction between DES-functionalized graphene and biological organelles in cells.[36] Interestingly, the functionalization using DESs significantly alleviated cytotoxicity levels of graphene against human breast cancer cell line (MCF-7), gastric cancer (AGS), and macrophage (RAW264.7) cell lines, with a higher IC_{50} (i.e., >200 μg/mL) compared with pristine graphene and oxidized graphene. Nevertheless, to date, there are no studies on the DOX loading capacity of DES-functionalized nanomaterials. Therefore, for the first time, this study reports on the DOX loading capacity of DES-functionalized graphene and its anticancer activities against MCF-7.

METHODOLOGIES

Preparation of DESs. Choline chloride (ChCl) (purity ≥98%) was purchased from Sigma-Aldrich. Glycerol (purity 99.8%) was obtained from R&M Chemicals. Sucrose and urea (purity ∼99.5%) were provided by Merck (Darmstadt, Germany). Potassium permanganate ($KMnO_4$) with a purity of 99% was purchased from Univar. Doxorubicin (hydrochloride) with a purity of ≥98% was obtained from Cayman Chemical. Synthesis of DES ChCl:sucrose:water (4:1:4) and DES ChCl:glycerol:water (1:2:1) was according to a previous report.[37] First, all solid chemicals listed in Table 1 were dried overnight in a vacuum oven (Memmert VO500, ThermoFisher) at 60 °C. Next, the salt and HBDs were mixed according to the given molar ratio at 70 °C via magnetic stirring until a homogeneous solution was achieved. The resulting mixture was then transferred into a well-sealed and dark (covered with aluminum foil) bottle.

Preparation of Oxidized Graphene and DES-Functionalized Graphene. Sixty-nanometer flakes of graphene nanoplatelets (Gr) were provided by Graphene Supermarket with a purity of 98.5%, a lateral particle size of 3−7 μm, an average thickness of 7 nm, and a specific surface area of <15 m^2/g. Oxidation and functionalization of Gr were performed as previously reported.[34] Briefly, pristine graphene (PrGr) was dried overnight at 100 °C under vacuum to remove impurities (e.g., water). Oxidized Gr (OxGr) was prepared as a graphene pretreatment prior to the subsequent functionalization process. The dried PrGr was oxidized using a 1.0 M $KMnO_4$ solution and sonicated using an ultrasonic bath at 70 °C for 3 h. OxGr was washed with distilled water several times and filtered using a PTFE membrane (pore size: 0.45 μm) and a vacuum pump until the filtrate solution became transparent and neutral (i.e., pH = 7). OxGr was collected and dried in a vacuum oven. In the functionalization procedure, the dried OxGr was mixed with DES and sonicated using an ultrasonic bath at 70 °C for 3 h. Similar to the oxidation procedure, the DES-functionalized Gr was subsequently washed with distilled water and filtered until a clear and neutral solution was obtained. The collected DES-functionalized Gr was then dried in the vacuum oven. Table 1 shows the composition and molar ratios of the DESs as well as the abbreviations used for the DES-functionalized Gr samples.

Table 1. List of Abbreviations for DES-Functionalized Graphene

type of DES				
salt	HBD	tertiary component	molar ratio	abbreviation
ChCl	sucrose	water	4:1:4	SWGr
ChCl	glycerol	water	1:2:1	GlyWGr

Physicochemical Characterization. Changes in morphology of the Gr samples were observed using a Quant FEG 450 field emission scanning electron microscope (FE-SEM). An energy dispersive X-ray (EDX) analysis using an Oxford Inca 400 spectrometer was conducted to determine surface elements of PrGr, OxGr, and DES-functionalized Gr samples. DES-functionalized Gr samples were analyzed by FTIR using a Perkin Elmer 1600 FTIR spectrometer. The samples were measured in the range of 450−4000 wavenumbers. Raman spectra were recorded using a Renishaw System 2000 Raman spectrometer under a wavelength of 514 nm. The surface area of the samples was analyzed from the nitrogen adsorption−desorption isotherm at 77 K based on the Brunauer−Emmett−Teller (BET) method using the automatic Micromeritics ASAP-2020, TRISTAR II 3020 Kr. X-ray diffraction (XRD) analysis also was performed.

Doxorubicin Loading. PrGr, OxGr, and DES-functionalized Gr samples were added to DMSO (100 μg/mL) and vortexed until completely dispersed. Next, 50 μg/mL DOX was dissolved in DMSO and vortexed. Both solutions were mixed and sonicated for 15 min using a Branson 2800 ultrasonic bath. Subsequently, the mixture was agitated at 28 °C for 12 h using an orbital shaker ES-20 (Grant-Bio, UK). Next, the mixture was centrifuged at 14 000 rpm for 30 min using an ultracentrifuge (Hermle Z233 MK-2, Lausanne). The pellet (i.e., DOX-loaded Gr) was collected, dried in a vacuum oven, and stored at −20 °C (Lab Dryer, Protech). The supernatant was measured at a wavelength of 480 nm using the Synergy HTX multimode reader (Biotek). Entrapment efficiency % (EE) and drug loading capacity % (DLC) were determined by measuring unbound drug in the supernatant at an absorbance peak of 480 nm and using eqs 1 and 2.[38]

DOI: 10.1021/acsomega.9b03709
ACS Omega 2020, 5, 1656−1668

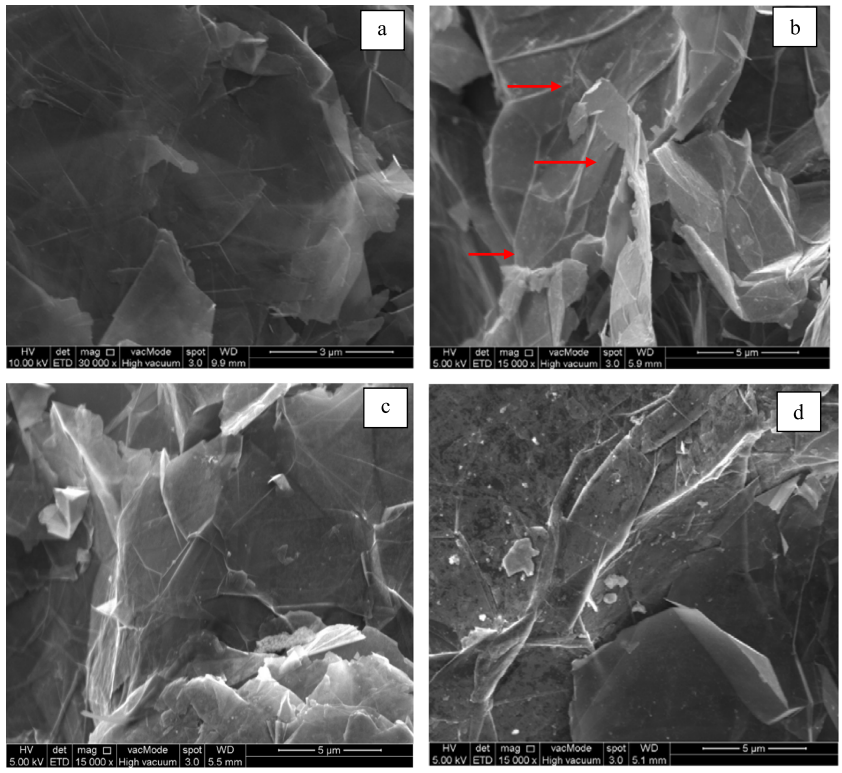

Figure 1. FE-SEM images of (a) PrGr, (b) OxGr, (c) SWGr, and (d) GlyWGr.

$$\text{EE}\ (\%) = (W_{\text{drug added}} - W_{\text{unbound drug}})/W_{\text{added drug}} \times 100 \quad (1)$$

$$\text{DLC}\ (\%) = (W_{\text{drug added}} - W_{\text{unbound drug}})/W_{\text{graphene}} \times 100 \quad (2)$$

where EE is the entrapment efficiency, DLC is the drug loading capacity, and W is the weight.

DOX-loaded graphene samples were labeled as follows: DOX-PrGr, DOX-OxGr, DOX-SWGr, and DOX-GlyWGr.

Cell Culture. The human breast cancer cell line MCF-7 was obtained from Cell Lines Service (Eppelgeim, Germany, 3000273), while macrophages (RAW264.7) were purchased from American Type Cell Collection (ATCC). MCF-7 was cultured in Roswell Park Memorial Institute (RPMI) medium supplemented with 10% heat inactivated fetal bovine serum (FBS) and a 1% mixture of streptomycin and penicillin. RAW264.7 cells were grown in Dulbecco's modified Eagle's medium (DMEM) supplemented with 10% FBS and 1% streptomycin and penicillin. Cells were incubated at 37 °C in a 5% CO_2 humidified incubator and were subcultured within 2−3 days.

Cell Viability. The 3-(4,5-dimethylthiazol-2-yl)-2,5-diphenyltetrazolium bromide (MTT) (Sigma-Aldrich) cell viability assay was performed according to the method of Hayyan et al.,[39] with slight modifications. First, the cells (1.5×10^4 per well) were seeded into 96-well plates (Corning) and incubated for 24 h at 37 °C in a 5% CO_2 humidified incubator. The DOX-loaded Gr samples were added the next day, followed by a 24 h incubation. Next, the supernatant was replaced with fresh medium (to avoid any interference), followed by addition of 2 mg/mL MTT reagent. After a 2 h incubation, the MTT reagent was discarded and later added with 100% DMSO. Absorbance was then measured at 570 nm. The percentage of cell viability was calculated with respect to untreated cells (eq 3). The 50% inhibitory concentration (IC_{50}) was determined using Graph Pad Prism 5 software.

$$\text{cell viability}\ (\%) = \left(\frac{a}{b}\right) \times 100 \quad (3)$$

where a is the absorbance of treated cells and b is the absorbance of untreated cells.

Cell Cycle Progression. The effects of DOX-loaded Gr samples on the cell cycle of MCF-7 cells were measured using a flow cytometer. After 24 h of treatment, cells were harvested then fixed with 70% cold ethanol, followed by overnight incubation at −80 °C. Next, cells were washed and suspended in phosphate-buffered saline (PBS). Cells were stained with 200 μL of propidium iodide/ribonuclease A (RNase A) for 1 h at 37 °C; then, the DNA content was evaluated using a flow cytometer (BD FACSCantoII).

Reactive Oxygen Species (ROS). Reactive oxygen species (ROS) generation was measured as previously described.[40] After cells were treated with DOX-loaded Gr samples for 24 h, dihydroethidium (DHE) dye was added into the live culture for 30 min. The cells were then fixed and washed with wash buffer (i.e., PBS). The percentage of cells with ROS were analyzed using the flow cytometer BD FACSCantoII (BD Biosciences).

Statistical Analysis. Values were expressed as mean ± standard deviation of three replicate measurements and were subjected to one-way analysis of variance (ANOVA). Significance differences were determined using the Duncan test at the 95% confidence level ($P < 0.05$). Analyses were performed using SigmaPlot 11.

RESULTS AND DISCUSSION

Physicochemical Characterization. Sample morphology was observed using FE-SEM to visualize the effect of DES

DOI: 10.1021/acsomega.9b03709
ACS Omega 2020, 5, 1656−1668

functionalization on the structure of the Gr samples. Figure 1 shows FE-SEM images of (a) PrGr, (b) OxGr, (c) SWGr, and (d) GlyWGr. As observed in Figure 1b, significant deformation occurred after oxidation of PrGr. These types of structural deformation may improve the dispersibility of Gr and can also be useful for the preparation of functionalization.[34] After functionalization of the DESs, the deformed structure of the OxGr disappeared. This suggests that Gr structure was restored by the addition of functional groups from the DESs. However, no significant difference between the structure of SWGr and GlyWGr was observed.

BET analysis was conducted for PrGr, OxGr, and DES-functionalized Gr to elucidate the effect of DES functionalization on the surface area of the Gr structure. Table 2 demonstrates a slight increase in the surface area of Gr after oxidation by $KMnO_4$, from 14.65 to 15.06 m^2/g. This is in accordance with the previous studies conducted on the oxidation of various carbon-based nanomaterials by different oxidizing agents.[41,42] However, smaller BET surface areas were observed after DES functionalization. This can be ascribed to the healing or recovering effects on the deformed structure of OxGr through the addition of functional groups, such as oxygen- and amine-containing functional groups. This supports the result of FE-SEM analysis where the deformed structure of the OxGr disappeared after DES functionalization.

Table 2. BET Surface Area of PrGr, OxGr, and DES-Functionalized Grs

sample	surface area (BET) m^2/g
PrGr	14.65
OxGr	15.06
SWGr	6.58
GlyWGr	8.09

As expected, carbon was the only surface element identified for PrGr in the EDX analysis (Table 3). Mild oxidation by $KMnO_4$ solution introduced new elements onto the surface of the Gr, including 4.73% oxygen (O), 0.46% potassium (K), and 2.99% manganese (Mn). Additional new surface elements appeared following SWGr and GlyWGr, i.e., chlorine (Cl) and nitrogen (N), which were not observed for unfunctionalized Gr samples (Table 3). This clearly can be ascribed to the use of ChCl-based DESs. In comparison with PrGr, the presence of these additional surface elements (i.e., O, K, Mn, Cl, and N) corroborated completion of the oxidation and DES functionalization processes. Hence, this also confirmed the presence of DES functional groups on the surface of Gr.

Table 3. EDX Surface Element Analysis of PrGr, OxGr, SWGr, and GlyWGr

	surface element, wt %					
sample	C	O	K	Mn	Cl	N
PrGr	100.00					
OxGr	91.84	4.73	0.46	2.99		
SWGr	95.79	3.79	0.07	0.21	0.07	0.07
GlyWGr	92.64	4.00	0.18	2.52	0.19	0.48

Significant changes in the FTIR spectra of Gr samples after DES functionalization were observed. Figure 2 shows that amine-based functional groups were detected in the GlyWGr and SWGr, including aliphatic isonitrile −N≡C stretching, aliphatic C-N stretching, aromatic isonitrile −N≡C stretching, NH_2 wagging and twisting, and secondary amide N-H wagging. DES-functionalized Grs also displayed several peaks that represented oxygen-based functional groups, such as O-H stretching, aliphatic aldehyde C═O stretching, C-O-H in-plane bending, and C-O stretching (Figure 2). As compared with a recent study from our group,[36] these amine- and oxygen-based functional groups were not identified in the FTIR spectra of PrGr. This is in good agreement with the EDX result that showed that additional surface elements such as N and O were introduced after functionalization with DES ChCl:glycerol:water (1:2:1) and ChCl:sucrose:water (4:1:4). These results suggested that DES functionalization may enhance the hydrophilicity of graphene through the introduction of additional functional groups such as amine- and oxygen-based functional groups. This is supported by previous studies[34,35] in which DES-functionalized carbon nanomaterials demonstrated better dispersion stability in aqueous media compared with unfunctionalized Gr.

A previous study[36] reported that the XRD pattern of PrGr contained several prominent peaks at 2θ = 26.33, 42.07, 44.62, 49.14, 54.19, and 72.69°, which indicate the crystalline planes (002), (100), (101), (012), (004), and (014), respectively. The same crystalline planes were observed in DES-functionalized Grs, which implied that the structural integrity of Gr was maintained even after DES functionalization (Figure 3). However, a significant shift was observed in the diffraction peaks identified on the XRD patterns of SWGr and GlyWGr (Table 4), especially for the crystalline planes (002) at 2θ = 26.33° that shifted to 26.63 and 26.61°, respectively. The peak intensities of Grs were also reduced for the crystalline planes (002), (100), (012), (004), and (014) after the oxidation and DES functionalization process (Table 4). As discussed in previous studies,[43−45] the same outcome was observed as effects of functionalization on the XRD patterns of the carbon nanomaterials.

Raman spectra of PrGr identified three distinguished peaks that represent 2D band (2700 cm^{-1}), G band (1580 cm^{-1}), and D band (1350 cm^{-1}).[36] The G band is essentially related to the formation of sp^2-bonded hybridized carbon, while the 2D band is generally associated with sp^3 hybridization of the graphitic structure.[46,47] The intensity I_D/I_G ratio of OxGr was significantly higher than that of PrGr (Table 5), which was due to the introduction of oxygenated functional groups after the oxidation process that increased structural deformation of Gr.[46] However, after DES functionalization, the I_D/I_G ratio was reduced, due to the increase in the intensity of the G band (Figure 4). This implied that the addition of functional groups by DES functionalization restored the sp^2 hybridization on the structure of Gr. As discussed previously, the FTIR spectra of DES-functionalized Grs confirmed the presence of new functional groups in SWGr and GlyWGr, especially amine-based functional groups that were not identified in PrGr and OxGr.

Doxorubicin Loading. To determine the amount of DOX loaded on the Gr samples, the amount of unbound DOX in solution was measured by an absorbance peak at 480 nm. Overall, all samples (i.e., PrGr, OxGr, and DES-functionalized Gr samples) interacted with DOX, as demonstrated by the decrease in the absorbance of DOX spectra after 12 h of incubation (Figure 5). A significant reduction in the spectra of absorption intensity of DOX was observed for SWGr and

DOI: 10.1021/acsomega.9b03709
ACS Omega 2020, 5, 1656−1668

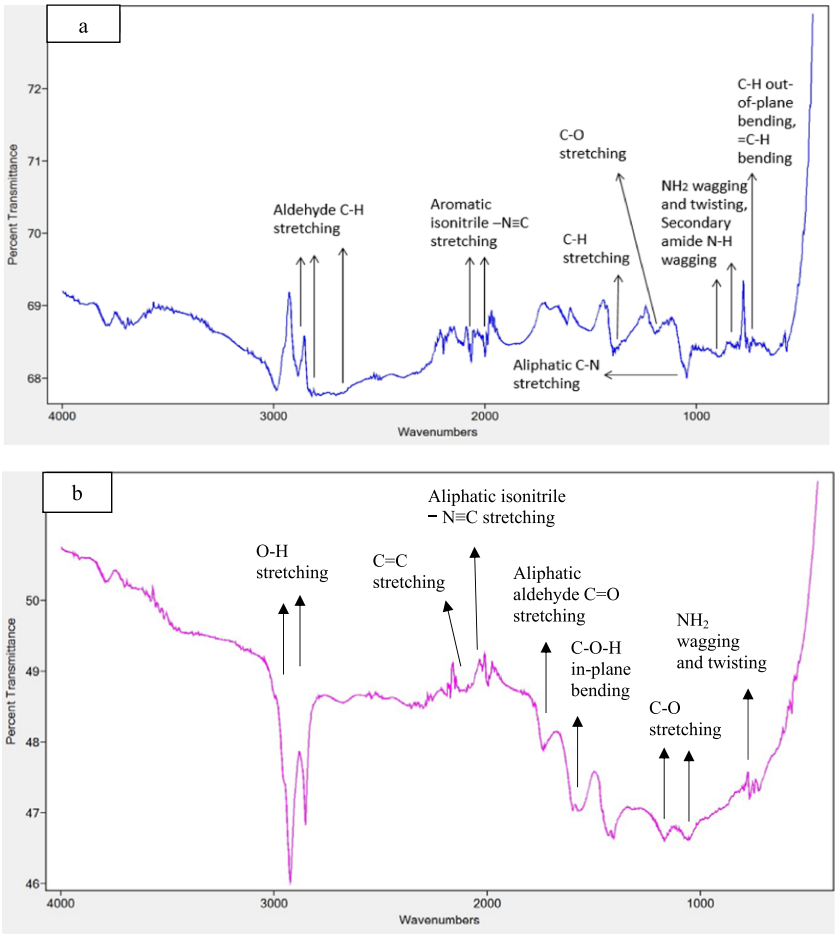

Figure 2. FTIR spectra of (a) GlyWGr and (b) SWGr.

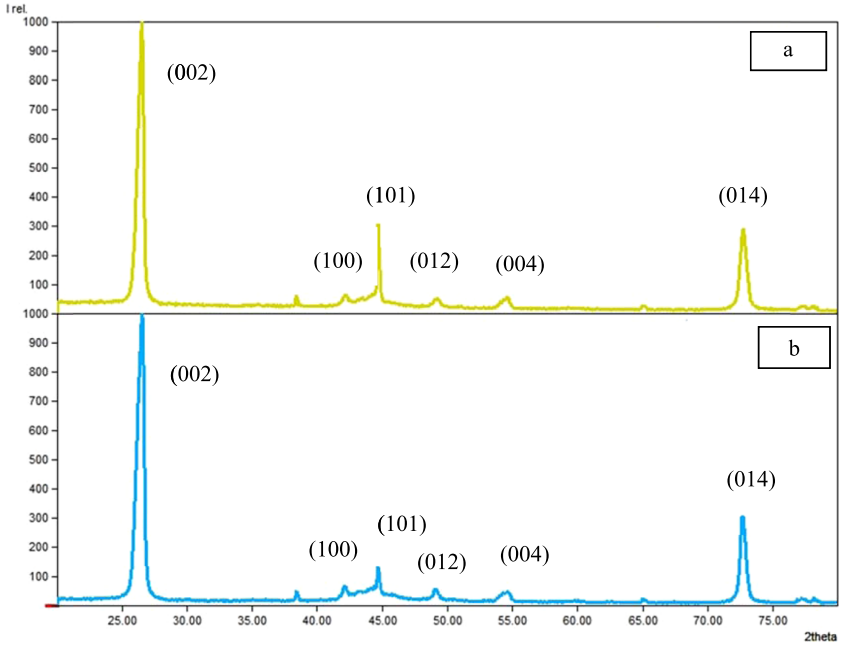

Figure 3. XRD pattern of (a) SWGr and (b) GlyWGr.

GlyWGr. This indicated the loading of DOX onto SWGr and GlyWGr was higher than PrGr and OxGr.

The EE and DLC using PrGr, OxGr, SWGr, and GlyWGr as DOX carriers were evaluated and are listed in Table 6. OxGr showed an insignificant difference compared with PrGr. The EE and DLC for both samples were approximately equivalent. On the other hand, the DES functionalization of Gr using ChCl:S:W and ChCl:Gly:W influenced the amount of DOX

DOI: 10.1021/acsomega.9b03709
ACS Omega 2020, 5, 1656−1668

Table 4. Diffraction Peaks Obtained from XRD Analysis of PrGr, OxGr, SWGr, and GlyWGr

	diffraction peak of (002)		diffraction peak of (100)		diffraction peak of (101)		diffraction peak of (012)		diffraction peak of (004)		diffraction peak of (014)	
sample	2θ (deg)	intensity	2θ (deg)	intensity	2θ (deg)	intensity	2θ (deg)	intensity	2θ (deg)	intensity	2θ (deg)	intensity
PrGr[36]	26.33	1000.0	42.07	94.9	44.62	172.8	49.14	65.4	54.19	35.7	72.69	459.7
OxGr[36]	26.59	1000.0	42.23	40.3	44.78	124.1	49.10	24.8	54.32	34.9	72.80	356.4
SWGr	26.63	1000.0	42.31	39.4	44.79	265.0	49.15	23.4	54.31	20.5	72.84	285.0
GlyWGr	26.61	1000.0	42.20	47.7	44.76	102.8	49.19	35.8	54.39	28.6	72.73	301.2

Table 5. Raman Spectra of PrGr, OxGR, SWGr, and GlyWGr

	G band		D band		2D band		
sample	P (cm^{-1})[a]	I[b]	P (cm^{-1})[a]	I[b]	P (cm^{-1})[a]	I[b]	I_D/I_G
PrGr[36]	1581.18	2687.46	1355.63	115.22	2726.07	1220.23	0.04
OxGr[36]	1581.09	1846.96	1356.92	254.20	2726.09	1077.98	0.14
SWGr	1579.85	850.98	1367.90	47.44	2724.80	505.94	0.06
GlyWGr	1579.68	845.44	1358.91	62.26	2727.38	478.97	0.07

[a]Position of Raman peak. [b]Intensity of Raman peak.

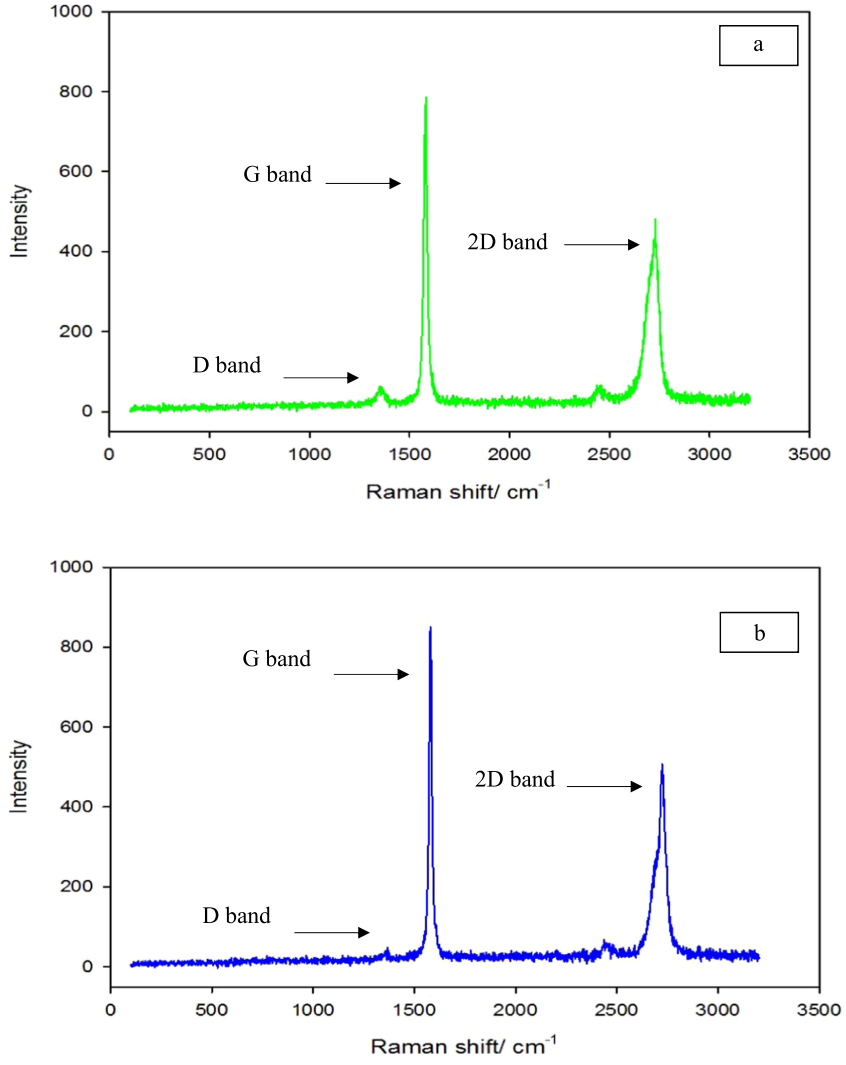

Figure 4. Raman spectra of (a) GlyWGr and (b) SWGr with identified peaks of 2D, G, and D bands.

loaded. This can be confirmed by significant increase of EE and DLC following both functionalization as compared with unfunctionalized Gr (i.e., PrGr and OxGr), Table 6. The use of SWGr as a DOX carrier exhibited the highest EE (51.84%) and DLC (25.92%), followed by GlyWGr (EE 51.04% and DLC 25.52%). Notably, the EE using both SWGr and GlyWGr was higher as compared to chitosan nanoparticle formulations, namely, Type B gelatin (EE: 8.4%), glucomannan (EE: 9.3%),

DOI: 10.1021/acsomega.9b03709
ACS Omega 2020, 5, 1656−1668

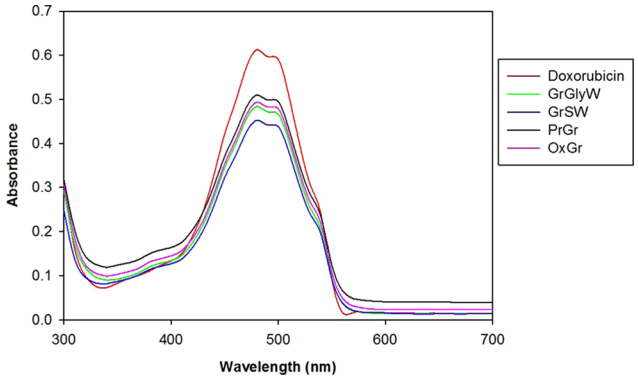

Figure 5. UV−vis spectra of doxorubicin solution (50 μg/mL) and mixture of doxorubicin (50 μg/mL) with Gr samples (100 μg/mL).

Table 6. Effect of Doxorubicin Loading on Entrapment Efficiency and Drug Loading Capacity for PrGr, OxGr, and DES-Functionalized Gr Samples

sample	entrapment efficiency (%)	drug loading capacity (%)
DOX-PrGr	39.98 ± 7.63	19.99 ± 3.81
DOX-OxGr	39.68 ± 5.71	19.84 ± 2.85
DOX-SWGr	51.84 ± 2.94	25.92 ± 1.47
DOX-GlyWGr	51.04 ± 1.44	25.52 ± 0.72

polyphosphoric acid (EE: 12.2%), and dextran sulfate-incorporated chitosan nanoparticles (EE: 21.9%).[48] In addition, the DLC using SWGr and GlyWGr was considerably higher in comparison to polymer micelle carrier systems such as poly(ethylene glycol)−poly(β-benzyl-L-aspartate) copolymer micelles that had a DLC ranging from 15 to 20%.[49] These DES-functionalized Gr systems also exhibited a higher DLC compared with glyceryl caprate-curdlan solid lipid nanoparticles (DLC of 2.8%).[50] Unlike other drug carriers, graphene is a superior nanodrug carrier, as both sides of a graphene sheet are accessible for drug loading/binding via a physical adsorption mechanism.[51,52] The presence of π electrons on graphitic domains promotes the formation of noncovalent binding via π-π stacking interactions with various compounds or substances, including DOX.[17,53−55] These π electrons on the plane immobilized DOX via noncovalent physical adsorption (physisorption).[15] In addition to the π−π electron stacking interactions, DES-functionalized Gr may also form strong hydrogen bonds with DOX. This is because the presence of DES functional groups on the surface of Gr may promote hydrogen-bonding interactions between DES-functionalized Gr and DOX.[56,57] The combined effect of these two interactions (i.e., π−π stacking and hydrogen bonding) may impart SWGr and GlyWGr with a higher drug loading capacity compared with unfunctionalized Gr. As shown by EDX analysis, SWGr and GlyWGr identified surface elements such as O and N permit the presence of functional groups that may form hydrogen bonds with DOX. This feature likely contributed to the higher DOX loading capacity of SWGr and GlyWGr.

Cytotoxicity Analysis. The cytotoxic effect of free loaded-Gr and DOX-loaded-Gr samples on cell viability was studied using the MTT cell viability assay, particularly with MCF-7 and RAW264.7 cell lines (Table 7). Table 7 shows that SWGr exhibited a lower IC_{50} than GlyWGr on both MCF-7 and RAW264.7 cells (284.20 and 363.03 μg/mL, respectively), indicating that the toxicity of SWGr was higher than that of GlyWGr (443.05 and 476.80 μg/mL, respectively). Compared with a previous study,[36] the toxicity of SWGr and GlyWGr for both MCF-7 and RAW264.7 cells was significantly lower than that of PrGr and OxGr. This implied that functionalization of graphene using DESs (i.e., ChCl:S:W and ChCl:Gly:W) was effective in reducing the cytotoxicity of graphene, especially using DES ChCl:Gly:W as a functionalizing agent.

Table 7. IC_{50} Values of Free Loaded-PrGr, -OxGr, -SWGr, and -GlyWGr, and DOX-Loaded-PrGr, -OxGr, -SWGr, and -GlyWGr on MCF-7 and RAW264.7 Cell Lines and also Their Selectivity Index

	IC_{50} (μg/mL)		
sample	RAW264.7	MCF-7	selectivity index
PrGr[36]	358.95 ± 2.35	161.70 ± 12.45	2.22
OxGr[36]	278.10 ± 2.00	117.25 ± 11.95	2.37
SWGr	363.03 ± 9.95	284.20 ± 7.27	1.28
GlyWGr	476.80 ± 1.69	443.05 ± 10.15	1.08
DOX-PrGr	291.00 ± 8.39	37.26 ± 4.33	7.81
DOX-OxGr	130.8 ± 4.81	26.49 ± 4.29	4.94
DOX-SWGr	234.87 ± 10.34	34.15 ± 4.82	6.88
DOX-GlyWGr	332.63 ± 4.95	61.46 ± 5.80	5.41

DOX-OxGr demonstrated the lowest IC_{50} toward MCF-7 (IC_{50} of 26.49 μg/mL), followed by the following sequence: DOX-SWGr (IC_{50} of 34.15 μg/mL) < DOX-PrGr (IC_{50} of 34.72 μg/mL) < DOX-GlyWGr (IC_{50} of 61.46 μg/mL) < SWGr (IC_{50} of 284.20 μg/mL) < GlyWGr (IC_{50} of 443.05 μg/mL). The same trend was observed with the RAW264.7 cell line, in which DOX-OxGr (IC_{50} of 130.8 μg/mL) exhibited the lowest IC_{50} compared with DOX-SWGr (IC_{50} of 234.87 μg/mL) < DOX-PrGr (IC_{50} of 300.75 μg/mL) < DOX-GlyWGr (IC_{50} of 332.63 μg/mL) < SWGr (IC_{50} of 363.03 μg/mL) < GlyWGr (IC_{50} of 476.80 μg/mL). The combined cytotoxic effect of OxGr and DOX was highly toxic toward both cells. Unlike DOX-loaded DES-functionalized Gr, the high cytotoxicity of DOX-OxGr against macrophage cells (i.e., RAW264.7 cells) is somehow unfavorable for the drug delivery system.

Compared with the free loaded-SWGr and -GlyWGr, there was a considerable increase in the toxicity of DOX-SWGr and DOX-GlyWGr compared with free loaded Gr (Table 7). The toxicity of these DOX-loaded-Gr samples was significantly higher compared with previous studies of free loaded Gr.[36,58] In comparison with other graphene-based DOX carriers, multifunctional graphene oxide drug carriers named GO/PEI.Ac-FI-PEG-LA at various concentrations (0.5, 1, 2, and 4 μM) exhibited higher cell inhibition than free loaded Gr (i.e., approximately 50% inhibition).[59] This higher toxicity of DOX-loaded Gr compared with free loaded Gr indicated that the lethal interaction between graphene and cells was significantly increased when DOX was loaded onto graphene. The significant detrimental effects of DOX-SWGr and DOX-GlyWGr also can be identified via optical microscopy at 40× and 100× magnification, as shown in Figure 6. Cell confluency was significantly reduced relative to untreated MCF-7. Changes in the size and morphology of MCF-7 were observed after being treated with DOX-SWGr and DOX-GlyWGr.

On the selectivity index of the nanocarriers, RAW264.7 cells were used as nontargeted cells due to the importance of macrophages in the immune system for human defense. The selectivity index was determined as the ratio of the sample's IC_{50} on cancerous cells over their IC_{50} on nontargeted cells. Table 7 shows that DOX-PrGr exhibited the highest selectivity

DOI: 10.1021/acsomega.9b03709
ACS Omega 2020, 5, 1656−1668

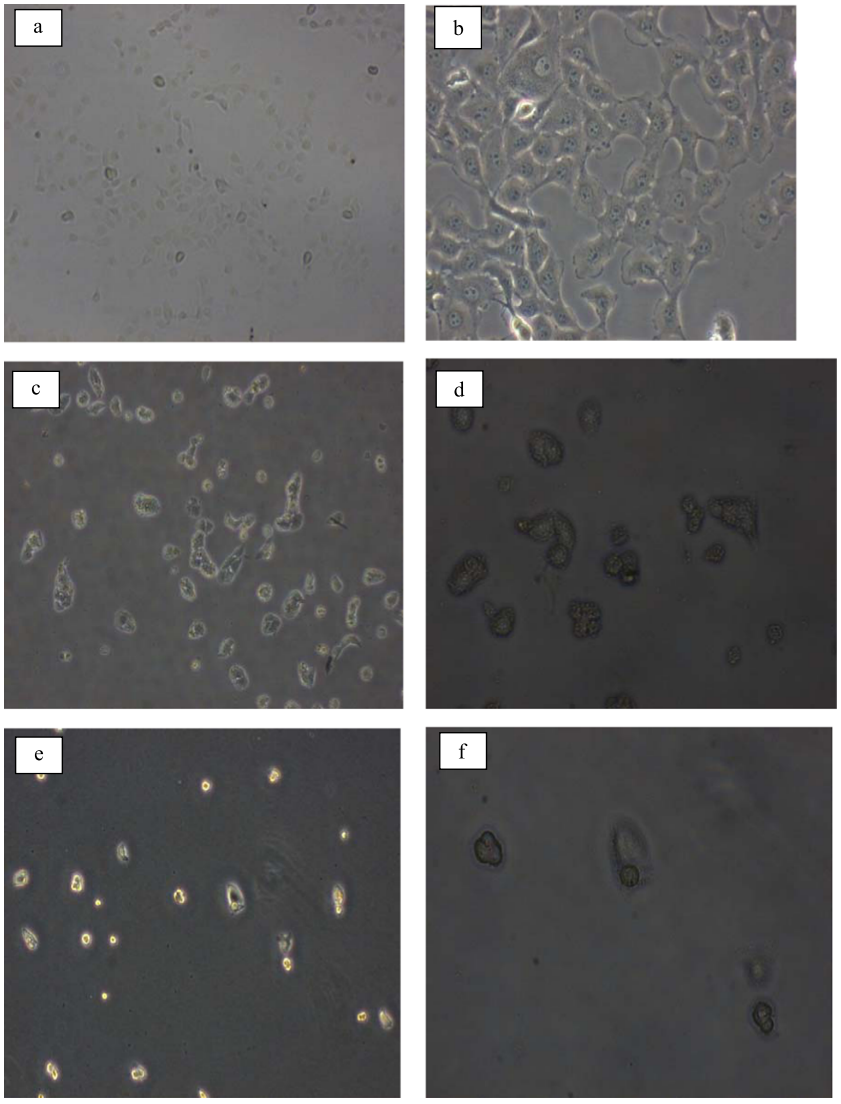

Figure 6. Untreated MCF-7 cells at (a) 40× and (b) 100× magnification, DOX-GlyWGr-treated MCF-7 at (c) 40× and (d) 100× magnification, and DOX-SWGr-treated MCF-7 at (e) 40× and (f) 100× magnification.

index against MCF-7 cells with 7.81, followed by DOX-SWGr (6.88), DOX-GlyWGr (5.41), and DOX-OxGr (4.94). The selectivity index of DOX-SWGr and DOX-GlyWGr was significantly increased compared with the free loaded-SWGr (1.28) and -GlyWGr (1.08). These levels of selectivity are considered to be significantly higher compared with other synthetic anticancer drugs, such as piperidinyl-diethylstilbestrol, pyrrolidinyl-diethylstilbestrol, alisiaquinol, and 4-hydroxy tamoxifen, which were reported to possess a selectivity index < 2.00.[60,61] Although DOX-PrGr showed higher selectivity against the MCF-7 cell line, its toxicity toward RAW264.7 cells was significantly high. The aforementioned high toxicity against macrophages is undesirable for anticancer drugs. Drugs that possess high cytotoxicity against macrophages may cause deterioration of the human immune system. Therefore, GlyWGr is a potential carrier for DOX that has mild cytotoxicity against macrophage cells.

Gr samples at their respective IC_{50} were tested in ROS and cell cycle analysis assays to further elucidate mechanisms of cell death after exposure to DOX-loaded Gr. The use of the IC_{50} concentration may better reflect cell death mechanisms, as 50% of the cells are inhibited at this concentration.

Reactive Oxygen Species (ROS) Generation. One of the cell death mechanisms caused by DOX involves the generation of ROS, which lead to cellular oxidative damage.[62−64] Previous studies[65,66] deconvoluted several mechanisms of DOX-mediated ROS stimulation, including one that involves an enzymatic pathway that is coupled with the mitochondrial respiratory chain and also a nonenzymatic mechanism that uses iron. Several enzymes, namely, NAD(P)H dehydrogenase, cytochrome p450, and nitric oxide synthase, have been speculated to initiate metabolic oxidation via the reductive effect of DOX.[67,68] In addition, DOX also may induce release of calcium from internal stores that leads to stimulation of ROS and interruption of cellular redox balance.[62]

Figure 7 demonstrates that the peaks shift to the right (i.e., greater fluorescence intensity), indicating an increase of ROS generation by all DOX-loaded-Gr samples compared with untreated cells. This indicates that the Gr samples were able to retain one of the DOX anticancer properties (i.e., ROS generation). This result is in agreement with poly(γ-benzyl-$_L$-glutamate)-*block*-hyaluronan (PBLG-*b*-HYA)-based polymersomes, which also retained the ROS generation behavior of

DOI: 10.1021/acsomega.9b03709
ACS Omega 2020, 5, 1656−1668

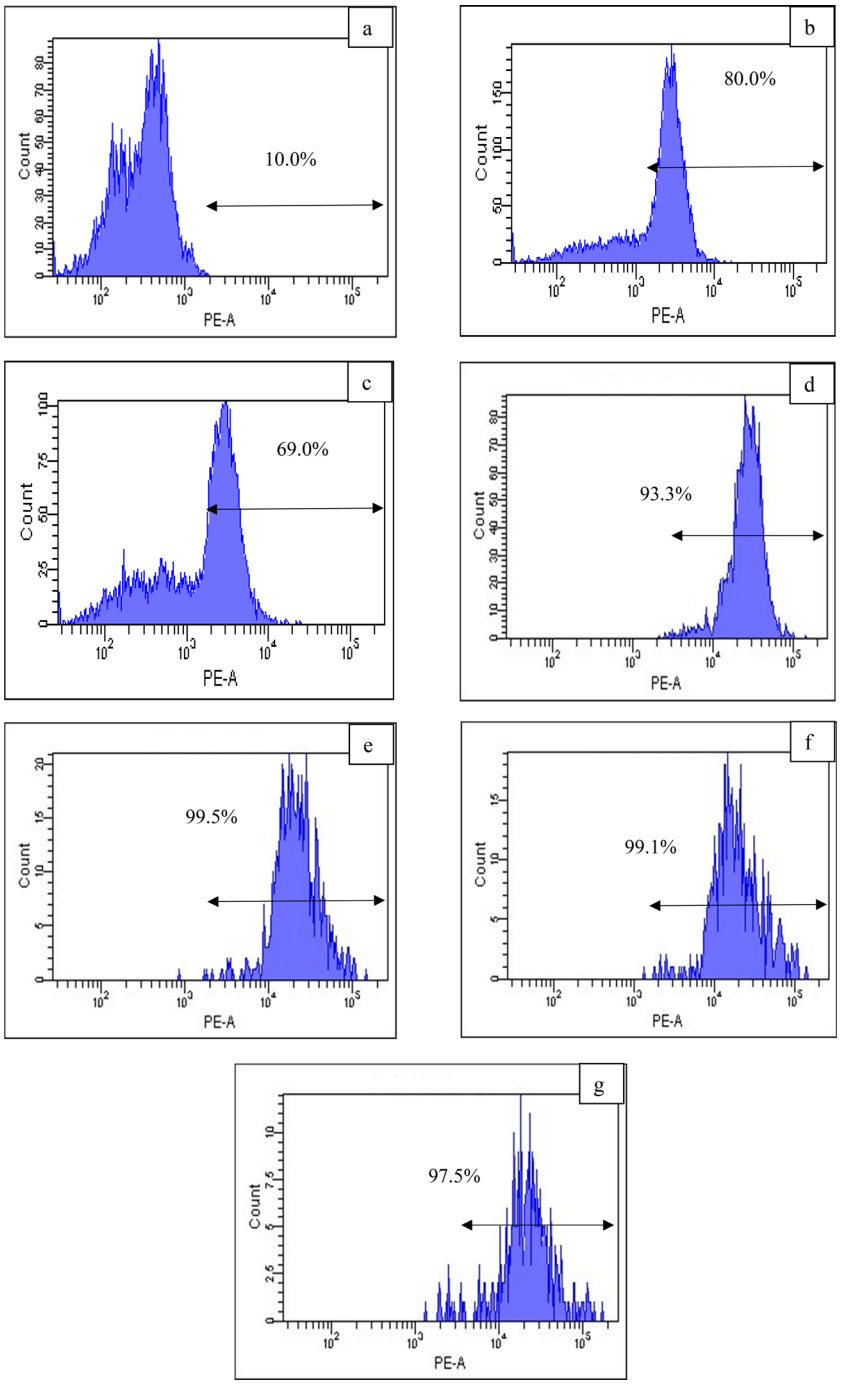

Figure 7. ROS generation of (a) untreated MCF-7 cells and (b) SWGr, (c) GlyWGr, (d) DOX-PrGr, (e) DOX-OxGr, (f) DOX-SWGr, and (g) DOX-GlyWGr-treated MCF-7. Data are representative of three independent experiments.

DOX.[69] DOX-OxGr possessed the highest level of ROS generation (99.3%) followed by DOX-GlyWGr (99.1%). DOX-loaded-Gr also exhibited higher ROS generation compared with free loaded-Gr (i.e., SWGr 80.0% and GlyWGr 69.0%). These levels of ROS generation were significantly higher compared with unloaded graphene samples from various graphene-based compounds, such as oxygenated graphene, aggregated graphene, graphene oxide, and nitric oxide-functionalized graphene.[70−73] This demonstrated that loading of DOX onto graphene increased intracellular ROS generation. These ROS generation results also aligned with the cell viability analysis, where DOX-OxGr and DOX-SWGr exhibited the most destructive effects toward MCF-7 cells compared with DOX-PrGr and DOX-GlyWGr. This confirms the role of DOX-induced ROS generation in cancer cell death was significant, which is in agreement with previous studies[63,74−76] regarding the critical role of ROS in anticancer activities toward various cancerous cells. For example, Tsang et al.[77] demonstrated that increased intracellular ROS generation, namely, superoxide and hydrogen peroxide, resulted in cell death of the human osteosarcoma cell line.

Cell Cycle Disruption. One of the strategies used for developing anticancer agents is modulating progression of the cell cycle. Therefore, propidium iodide staining and flow

DOI: 10.1021/acsomega.9b03709
ACS Omega 2020, 5, 1656−1668

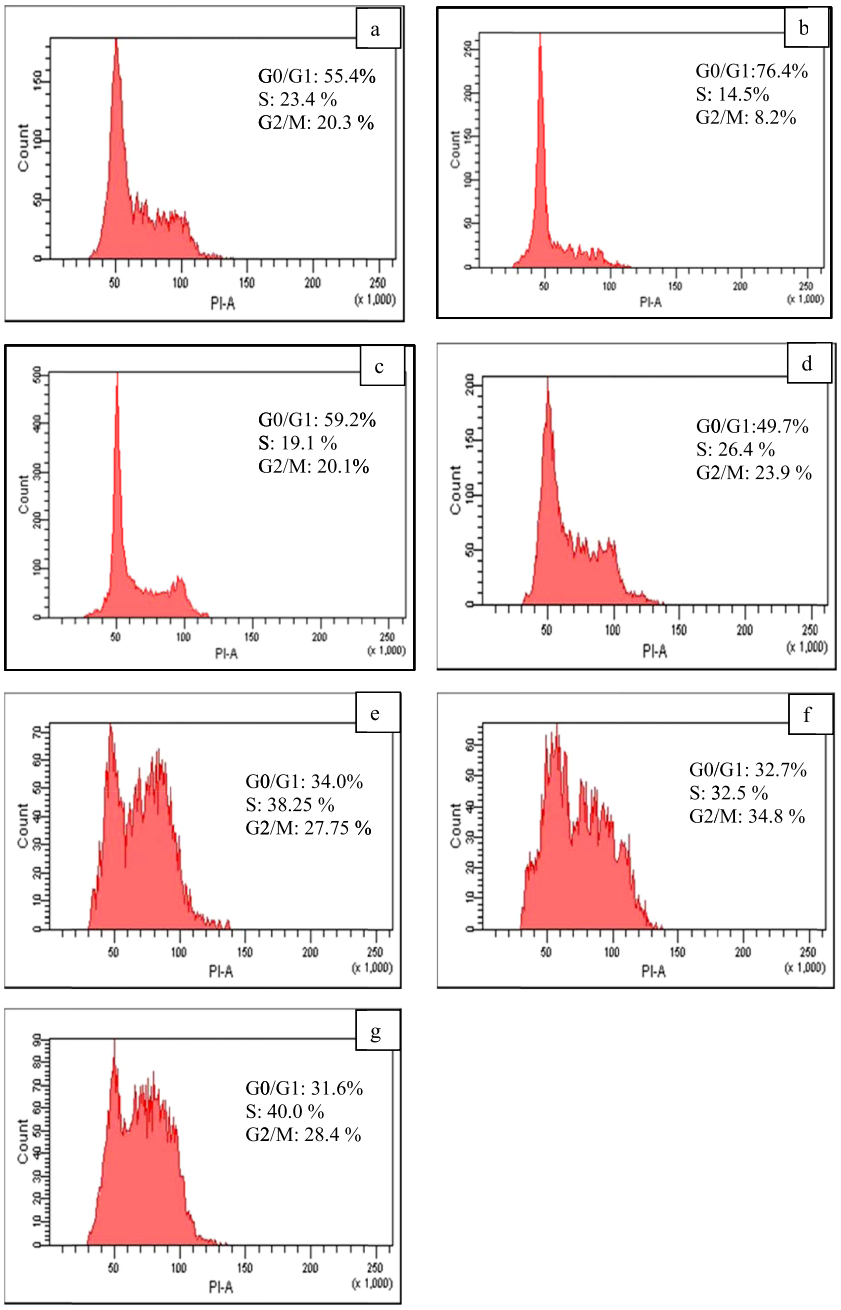

Figure 8. Cell cycle comparison of the (a) untreated MCF-7 cells and (b) SWGr, (c) GlyWGr, (d) DOX-PrGr, (e) DOX-OxGr, (f) DOX-SWGr, and (g) DOX-GlyWGr-treated MCF-7. Data are representative of three independent experiments.

cytometry analysis of the treated MCF-7 cells was conducted to elucidate the impact of DOX-loaded-Gr on cell cycle phases. Figure 8 shows that free loaded Gr and DOX-loaded-Gr (i.e., PrGr, OxGr, SWGr, and GlyWGr) disrupted cell cycle progression of the MCF-7 cell line. Untreated MCF-7 cells (as a control) had 55.4% of their cell population in G0/G1 phase, 23.4% in S phase, and 20.3% in G2/M phase. SWGr and GlyWGr mildly disrupted progression of the cell cycle (Figure 8). On the other hand, DOX-loaded-PrGr, -OxGr, -SWGr, and -GlyWGr arrested the cells at S phase and G2/M phase (i.e., increased the number of cells at S phase and G2/M phase) and consequently impeded cell cycle progression. Significant cell arrest at S phase and G2/M phase was observed with DOX-GlyWGr, with 40% of the cell population at S phase and 28.4% at G2/M phase, compared with untreated MCF-7 cells (i.e., S phase: 23.4% and G2/M phase: 20.3% of the cell population). As shown in Figure 9, the G2 checkpoint permits the cells to repair DNA damage before proceeding into the mitosis phase. The significant amount of DNA damage that occurs in the cells may lead to a higher number of cells arrested at the G2/M phase. DOX-induced DNA damage is believed to predominantly occur at the G2/M phase.[78] Cell arrest at the G2/M checkpoint may cause cancer cells to undergo apoptosis and subsequently increase the destructive effects. This incident is in accordance with previous studies[79,80] of various types of cancer cell lines. The results also showed an obvious relationship between ROS and cell cycle mechanisms in which the increase of intracellular ROS by DOX-loaded Gr led to disruption of cell cycle progression. As studied previously,[64,81,82] a high level

DOI: 10.1021/acsomega.9b03709
ACS Omega 2020, 5, 1656−1668

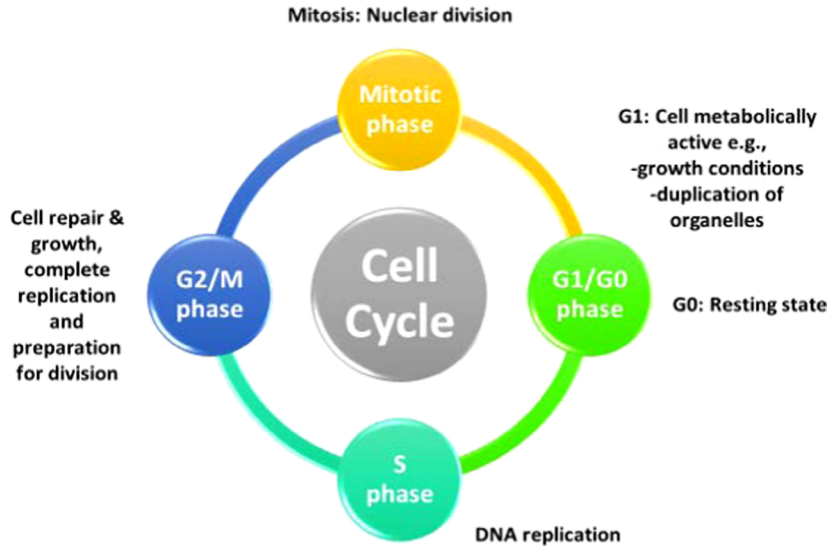

Figure 9. Diagrammatic representation of cell cycle phases.

of ROS can cause cell cycle arrest and apoptosis, especially for DOX-mediated cell death.

CONCLUSIONS

This study confirmed that DES-functionalized graphene samples (i.e., SWGr and GlyWGr) were able to increase the DOX loading capacity compared with PrGr and OxGR. This was due to surface modification of Gr by DESs ChCl:S:W and ChCl:Gly:W. After DOX loading, the drug-loaded-Grs (i.e., DOX-SWGr and DOX-GlyWGr) were more toxic against MCF-7 cells than free loaded-Gr (i.e., SWGr and GlyWGr). However, DOX-SWGr exhibited higher anticancer activity (IC_{50} of 34.15 μg/mL) and higher selectivity (index value of 6.88) against MCF-7 cells compared with DOX-GlyWGr (IC_{50} of 61.46 μg/mL, index value of 5.41). DOX-SWGr and DOX-GlyWGr also had destructive effects against the MCF-7 cell line through the generation of intracellular ROS and cell cycle disruption. Overall, SWGr and GlyWGr represented promising nanocarriers for DOX because of their high toxicity against breast cancer cells.

AUTHOR INFORMATION

Corresponding Authors

*E-mail: maan_hayyan@yahoo.com, mhayyan@muscatuniversity.edu.om (M.H.).

*E-mail: ngoh@um.edu.my. Tel./Fax: +6-03-7967-5311 (G.C.N.).

ORCID

Maan Hayyan: 0000-0002-2179-0801

Notes

The authors declare no competing financial interest.

ACKNOWLEDGMENTS

The authors would like to express their gratitude to the University of Malaya Grant no. IIRG010C-2019 and to Malaysian Toray Science Foundation (MTSF) for their support to this research.

REFERENCES

(1) Nawara, K.; Romiszewski, J.; Kijewska, K.; Szczytko, J.; Twardowski, A.; Mazur, M.; Krysinski, P. Adsorption of Doxorubicin onto Citrate-Stabilized Magnetic Nanoparticles. *J. Phys. Chem. C* **2012**, *116*, 5598−5609.

(2) Cortés-Funes, H.; Coronado, C. Role of anthracyclines in the era of targeted therapy. *Cardiovasc. Toxicol.* **2007**, *7*, 56−60.

(3) Shi, J.; Kantoff, P. W.; Wooster, R.; Farokhzad, O. C. Cancer nanomedicine: progress, challenges and opportunities. *Nat. Rev. Cancer* **2017**, *17*, 20.

(4) Chittasupho, C.; Lirdprapamongkol, K.; Kewsuwan, P.; Sarisuta, N. Targeted delivery of doxorubicin to A549 lung cancer cells by CXCR4 antagonist conjugated PLGA nanoparticles. *Eur. J. Pharm. Biopharm.* **2014**, *88*, 529−538.

(5) Biswas, S.; Dodwadkar, N. S.; Deshpande, P. P.; Parab, S.; Torchilin, V. P. Surface functionalization of doxorubicin-loaded liposomes with octa-arginine for enhanced anticancer activity. *Eur. J. Pharm. Biopharm.* **2013**, *84*, 517−525.

(6) Zhao, N.; Woodle, M. C.; Mixson, A. J. Advances in delivery systems for doxorubicin. *J. Nanomed. Nanotechnol.* **2018**, *9*, 519.

(7) Shah, N. H.; Carvajal, M. T.; Patel, C. I.; Infeld, M. H.; Malick, A. W. Self-emulsifying drug delivery systems (SEDDS) with polyglycolyzed glycerides for improving in vitro dissolution and oral absorption of lipophilic drugs. *Int. J. Pharm.* **1994**, *106*, 15−23.

(8) Sharma, A.; Sharma, U. S. Liposomes in drug delivery: Progress and limitations. *Int. J. Pharm.* **1997**, *154*, 123−140.

(9) Khaled, S. A.; Burley, J. C.; Alexander, M. R.; Yang, J.; Roberts, C. J. 3D printing of tablets containing multiple drugs with defined release profiles. *Int. J. Pharm.* **2015**, *494*, 643−650.

(10) Zhang, H.; Li, Q.; Liu, R.; Zhang, X.; Li, Z.; Luan, Y. A Versatile Prodrug Strategy to In Situ Encapsulate Drugs in MOF Nanocarriers: A Case of Cytarabine-IR820 Prodrug Encapsulated ZIF-8 toward Chemo-Photothermal Therapy. *Adv. Funct. Mater.* **2018**, *28*, No. 1802830.

(11) Liu, Z.; Jiao, Y.; Wang, Y.; Zhou, C.; Zhang, Z. Polysaccharides-based nanoparticles as drug delivery systems. *Adv. Drug Delivery Rev.* **2008**, *60*, 1650−1662.

(12) Chen, K. H.; Ling, Y. Z.; Cao, C.; Li, X. Y.; Chen, X.; Wang, X. Y. Chitosan derivatives/reduced graphene oxide/alginate beads for small-molecule drug delivery. *Mater. Sci. Eng., C* **2016**, *69*, 1222−1228.

(13) Bitounis, D.; Ali-Boucetta, H.; Hong, B. H.; Min, D.-H.; Kostarelos, K. Prospects and Challenges of Graphene in Biomedical Applications. *Adv. Mater.* **2013**, *25*, 2258−2268.

(14) Zhu, Y.; Murali, S.; Cai, W.; Li, X.; Suk, J. W.; Potts, J. R.; Ruoff, R. S. Graphene and Graphene Oxide: Synthesis, Properties, and Applications. *Adv. Mater.* **2010**, *22*, 3906−3924.

DOI: 10.1021/acsomega.9b03709
ACS Omega 2020, 5, 1656−1668

(15) Liu, J.; Cui, L.; Losic, D. Graphene and graphene oxide as new nanocarriers for drug delivery applications. *Acta Biomater.* **2013**, *9*, 9243−9257.
(16) Goenka, S.; Sant, V.; Sant, S. Graphene-based nanomaterials for drug delivery and tissue engineering. *J. Controlled Release* **2014**, *173*, 75−88.
(17) Yang, K.; Feng, L.; Shi, X.; Liu, Z. Nano-graphene in biomedicine: theranostic applications. *Chem. Soc. Rev.* **2013**, *42*, 530−547.
(18) de Melo-Diogo, D.; Costa, E. C.; Alves, C. G.; Lima-Sousa, R.; Ferreira, P.; Louro, R. O.; Correia, I. J. POxylated graphene oxide nanomaterials for combination chemo-phototherapy of breast cancer cells. *Eur. J. Pharm. Biopharm.* **2018**, *131*, 162−169.
(19) Zhang, Y.; Ali, S. F.; Dervishi, E.; Xu, Y.; Li, Z.; Casciano, D.; Biris, A. S. Cytotoxicity Effects of Graphene and Single-Wall Carbon Nanotubes in Neural Phaeochromocytoma-Derived PC12 Cells. *ACS Nano* **2010**, *4*, 3181−3186.
(20) McCallion, C.; Burthem, J.; Rees-Unwin, K.; Golovanov, A.; Pluen, A. Graphene in therapeutics delivery: Problems, solutions and future opportunities. *Eur. J. Pharm. Biopharm.* **2016**, *104*, 235−250.
(21) Bottari, G.; Herranz, M. A.; Wibmer, L.; Volland, M.; Rodriguez-Perez, L.; Guldi, D. M.; Hirsch, A.; Martin, N.; D'Souza, F.; Torres, T. Chemical functionalization and characterization of graphene-based materials. *Chem. Soc. Rev.* **2017**, 4464.
(22) Martínez, M. T.; Callejas, M. A.; Benito, A. M.; Cochet, M.; Seeger, T.; Ansón, A.; Schreiber, J.; Gordon, C.; Marhic, C.; Chauvet, O.; Maser, W. K. Modifications of single-wall carbon nanotubes upon oxidative purification treatments. *Nanotechnology* **2003**, *14*, 691.
(23) Georgakilas, V.; Kordatos, K.; Prato, M.; Guldi, D. M.; Holzinger, M.; Hirsch, A. Organic Functionalization of Carbon Nanotubes. *J. Am. Chem. Soc.* **2002**, *124*, 760−761.
(24) Georgakilas, V.; Otyepka, M.; Bourlinos, A. B.; Chandra, V.; Kim, N.; Kemp, K. C.; Hobza, P.; Zboril, R.; Kim, K. S. Functionalization of Graphene: Covalent and Non-Covalent Approaches, Derivatives and Applications. *Chem. Rev.* **2012**, *112*, 6156−6214.
(25) Liu, Z.; Robinson, J. T.; Sun, X.; Dai, H. PEGylated nanographene oxide for delivery of water-insoluble cancer drugs. *J. Am. Chem. Soc.* **2008**, *130*, 10876−7.
(26) Park, J.; Fong, P. M.; Lu, J.; Russell, K. S.; Booth, C. J.; Saltzman, W. M.; Fahmy, T. M. PEGylated PLGA nanoparticles for the improved delivery of doxorubicin. *Nanomedicine* **2009**, *5*, 410−418.
(27) Abbott, A. P.; Boothby, D.; Capper, G.; Davies, D. L.; Rasheed, R. K. Deep eutectic solvents formed between choline chloride and carboxylic acids: versatile alternatives to ionic liquids. *J. Am. Chem. Soc.* **2004**, *126*, 9142−9147.
(28) Smith, E. L.; Abbott, A. P.; Ryder, K. S. Deep Eutectic Solvents (DESs) and Their Applications. *Chem. Rev.* **2014**, *114*, 11060−11082.
(29) Jhong, H.-R.; Wong, D. S.-H.; Wan, C.-C.; Wang, Y.-Y.; Wei, T.-C. A novel deep eutectic solvent-based ionic liquid used as electrolyte for dye-sensitized solar cells. *Electrochem. Commun.* **2009**, *11*, 209−211.
(30) Zainal-Abidin, M. H.; Hayyan, M.; Hayyan, A.; Jayakumar, N. S. New horizons in the extraction of bioactive compounds using deep eutectic solvents: A review. *Anal. Chim. Acta* **2017**, *979*, 1−23.
(31) Nkuku, C. A.; LeSuer, R. J. Electrochemistry in deep eutectic solvents. *J. Phys. Chem. B* **2007**, *111*, 13271−7.
(32) Morrison, H. G.; Sun, C. C.; Neervannan, S. Characterization of thermal behavior of deep eutectic solvents and their potential as drug solubilization vehicles. *Int. J. Pharm.* **2009**, *378*, 136−139.
(33) Aroso, I. M.; Silva, J. C.; Mano, F.; Ferreira, A. S.; Dionísio, M.; Sá-Nogueira, I.; Barreiros, S.; Reis, R. L.; Paiva, A.; Duarte, A. R. C. Dissolution enhancement of active pharmaceutical ingredients by therapeutic deep eutectic systems. *Eur. J. Pharm. Biopharm.* **2016**, *98*, 57−66.
(34) Hayyan, M.; Abo-Hamad, A.; AlSaadi, M. A.; Hashim, M. A. Functionalization of graphene using deep eutectic solvents. *Nanoscale Res. Lett.* **2015**, *10*, 324.
(35) Abo-Hamad, A.; Hayyan, M.; AlSaadi, M. A.; Mirghani, M. E. S.; Hashim, M. A. Functionalization of carbon nanotubes using eutectic mixtures: A promising route for enhanced aqueous dispersibility and electrochemical activity. *Chem. Eng. J.* **2017**, *311*, 326−339.
(36) Zainal-Abidin, M. H.; Hayyan, M.; Ngoh, G. C.; Wong, W. F. From nanoengineering to nanomedicine: A facile route to enhance biocompatibility of graphene as a potential nano-carrier for targeted drug delivery using natural deep eutectic solvents. *Chem. Eng. Sci.* **2019**, *195*, 95−106.
(37) Hayyan, M.; Mbous, Y. P.; Looi, C. Y.; Wong, W. F.; Hayyan, A.; Salleh, Z.; Mohd-Ali, O. Natural deep eutectic solvents: cytotoxic profile. *SpringerPlus* **2016**, *5*, 1.
(38) How, C. W.; Rasedee, A.; Manickam, S.; Rosli, R. Tamoxifen-loaded nanostructured lipid carrier as a drug delivery system: Characterization, stability assessment and cytotoxicity. *Colloids Surf., B* **2013**, *112*, 393−399.
(39) Hayyan, M.; Looi, C. Y.; Hayyan, A.; Wong, W. F.; Hashim, M. A. In Vitro and In Vivo toxicity profiling of ammonium-based deep eutectic solvents. *PLoS One* **2015**, *10*, No. e0117934.
(40) Hajrezaie, M.; Paydar, M.; Looi, C. Y.; Moghadamtousi, S. Z.; Hassandarvish, P.; Salga, M. S.; Karimian, H.; Shams, K.; Zahedifard, M.; Majid, N. A.; Ali, H. M.; Abdulla, M. A. Apoptotic effect of novel Schiff Based CdCl2(C14H21N3O2) complex is mediated via activation of the mitochondrial pathway in colon cancer cells. *Sci. Rep.* **2015**, *5*, 9097.
(41) Pifferi, V.; Cappelletti, G.; Di Bari, C.; Meroni, D.; Spadavecchia, F.; Falciola, L. Multi-Walled Carbon Nanotubes (MWCNTs) modified electrodes: Effect of purification and functionalization on the electroanalytical performances. *Electrochim. Acta* **2014**, *146*, 403−410.
(42) Dongil, A. B.; Bachiller-Baeza, B.; Guerrero-Ruiz, A.; Rodríguez-Ramos, I.; Martínez-Alonso, A.; Tascón, J. M. D. Surface chemical modifications induced on high surface area graphite and carbon nanofibers using different oxidation and functionalization treatments. *J. Colloid Interface Sci.* **2011**, *355*, 179−189.
(43) Talaeemashhadi, S.; Sansotera, M.; Gambarotti, C.; Famulari, A.; Bianchi, C. L.; Antonio Guarda, P.; Navarrini, W. Functionalization of multi-walled carbon nanotubes with perfluoropolyether peroxide to produce superhydrophobic properties. *Carbon* **2013**, *59*, 150−159.
(44) Wang, X.; Xing, W.; Song, L.; Yu, B.; Hu, Y.; Yeoh, G. H. Preparation of UV-curable functionalized graphene/polyurethane acrylate nanocomposite with enhanced thermal and mechanical behaviors. *React. Funct. Polym.* **2013**, *73*, 854−858.
(45) Hamwi, A.; Alvergnat, H.; Bonnamy, S.; Béguin, F. Fluorination of carbon nanotubes. *Carbon* **1997**, *35*, 723−728.
(46) Ferrari, A. C.; Meyer, J. C.; Scardaci, V.; Casiraghi, C.; Lazzeri, M.; Mauri, F.; Piscanec, S.; Jiang, D.; Novoselov, K. S.; Roth, S.; Geim, A. K. Raman Spectrum of Graphene and Graphene Layers. *Phys. Rev. Lett.* **2006**, *97*, No. 187401.
(47) Prolongo, S. G.; Jimenez-Suarez, A.; Moriche, R.; Ureña, A. In situ processing of epoxy composites reinforced with graphene nanoplatelets. *Compos. Sci. Technol.* **2013**, *86*, 185−191.
(48) Janes, K. A.; Fresneau, M. P.; Marazuela, A.; Fabra, A.; Alonso, M. aJ. Chitosan nanoparticles as delivery systems for doxorubicin. *J. Controlled Release* **2001**, *73*, 255−267.
(49) Kataoka, K.; Matsumoto, T.; Yokoyama, M.; Okano, T.; Sakurai, Y.; Fukushima, S.; Okamoto, K.; Kwon, G. S. Doxorubicin-loaded poly(ethylene glycol)−poly(β-benzyl-l-aspartate) copolymer micelles: their pharmaceutical characteristics and biological significance. *J. Controlled Release* **2000**, *64*, 143−153.
(50) Subedi, R. K.; Kang, K. W.; Choi, H.-K. Preparation and characterization of solid lipid nanoparticles loaded with doxorubicin. *Eur. J. Pharm. Sci.* **2009**, *37*, 508−513.
(51) Bao, H.; Pan, Y.; Ping, Y.; Sahoo, N. G.; Wu, T.; Li, L.; Li, J.; Gan, L. H. Chitosan-Functionalized Graphene Oxide as a Nanocarrier for Drug and Gene Delivery. *Small* **2011**, *7*, 1569−1578.

DOI: 10.1021/acsomega.9b03709
ACS Omega 2020, 5, 1656−1668

(52) Rana, V. K.; Choi, M.-C.; Kong, J.-Y.; Kim, G. Y.; Kim, M. J.; Kim, S.-H.; Mishra, S.; Singh, R. P.; Ha, C.-S. Synthesis and Drug-Delivery Behavior of Chitosan-Functionalized Graphene Oxide Hybrid Nanosheets. *Macromol. Mater. Eng.* **2011**, *296*, 131−140.
(53) Wang, Y.; Li, Z.; Wang, J.; Li, J.; Lin, Y. Graphene and graphene oxide: biofunctionalization and applications in biotechnology. *Trends Biotechnol.* **2011**, *29*, 205−212.
(54) Feng, L.; Wu, L.; Qu, X. New Horizons for Diagnostics and Therapeutic Applications of Graphene and Graphene Oxide. *Adv. Mater.* **2013**, *25*, 168−186.
(55) Gonçalves, G.; Vila, M.; Portolés, M.-T.; Vallet-Regi, M.; Gracio, J.; Marques, P. A. A. P. Nano-Graphene Oxide: A Potential Multifunctional Platform for Cancer Therapy. *Adv. Healthcare Mater.* **2013**, *2*, 1072−1090.
(56) Yang, X.; Zhang, X.; Liu, Z.; Ma, Y.; Huang, Y.; Chen, Y. High-Efficiency Loading and Controlled Release of Doxorubicin Hydrochloride on Graphene Oxide. *J. Phys. Chem. C* **2008**, *112*, 17554−17558.
(57) Depan, D.; Shah, J.; Misra, R. D. K. Controlled release of drug from folate-decorated and graphene mediated drug delivery system: Synthesis, loading efficiency, and drug release response. *Mater. Sci. Eng., C* **2011**, *31*, 1305−1312.
(58) Chang, Y.; Yang, S. T.; Liu, J. H.; Dong, E.; Wang, Y.; Cao, A.; Liu, Y.; Wang, H. In vitro toxicity evaluation of graphene oxide on A549 cells. *Toxicol. Lett.* **2011**, *200*, 201−10.
(59) Lv, Y.; Tao, L.; Annie Bligh, S. W.; Yang, H.; Pan, Q.; Zhu, L. Targeted delivery and controlled release of doxorubicin into cancer cells using a multifunctional graphene oxide. *Mater. Sci. Eng., C* **2016**, *59*, 652−660.
(60) Desoubzdanne, D.; Marcourt, L.; Raux, R.; Chevalley, S.; Dorin, D.; Doerig, C.; Valentin, A.; Ausseil, F.; Debitus, C. Alisiaquinones and alisiaquinol, dual inhibitors of Plasmodium falciparum enzyme targets from a New Caledonian deep water sponge. *J. Nat. Prod.* **2008**, *71*, 1189−92.
(61) Badisa, R. B.; Darling-Reed, S. F.; Joseph, P.; Cooperwood, J. S.; Latinwo, L. M.; Goodman, C. B. Selective Cytotoxic Activities of Two Novel Synthetic Drugs on Human Breast Carcinoma MCF-7 Cells. *Anticancer Res.* **2009**, *29*, 2993−2996.
(62) Kim, S.-Y.; Kim, S.-J.; Kim, B.-J.; Rah, S.-Y.; Chung, S. M.; Im, M.-J.; Kim, U.-H. Doxorubicin-induced reactive oxygen species generation and intracellular Ca2+increase are reciprocally modulated in rat cardiomyocytes. *Exp. Mol. Med.* **2006**, *38*, 535.
(63) Minotti, G.; Menna, P.; Salvatorelli, E.; Cairo, G.; Gianni, L. Anthracyclines: Molecular Advances and Pharmacologic Developments in Antitumor Activity and Cardiotoxicity. *Pharmacol. Rev.* **2004**, *56*, 185−229.
(64) Lau, A. T.; Wang, Y.; Chiu, J. F. Reactive oxygen species: current knowledge and applications in cancer research and therapeutic. *J. Cell. Biochem.* **2008**, *104*, 657−667.
(65) Gutierrez, P. L. The role of NAD(P)H oxidoreductase (DT-Diaphorase) in the bioactivation of quinone-containing antitumor agents: a review. *Free Radic. Biol. Med.* **2000**, *29*, 263−275.
(66) Shadle, S. E.; Bammel, B. P.; Cusack, B. J.; Knighton, R. A.; Olson, S. J.; Mushlin, P. S.; lson, R. D. O. Daunorubicin cardiotoxicity: Evidence for the importance of the quinone moiety in a free-radical-independent mechanism. *Biochem. Pharmacol.* **2000**, *60*, 1435−1444.
(67) Childs, A. C.; Phaneuf, S. L.; Dirks, A. J.; Phillips, T.; Leeuwenburgh, C. Doxorubicin Treatment in vivo Causes Cytochrome Release and Cardiomyocyte Apoptosis, As Well As Increased Mitochondrial Efficiency, Superoxide Dismutase Activity, and Bcl-2:Bax Ratio. *Cancer Res.* **2002**, *62*, 4592−4598.
(68) Doroshow, J. H.; Davies, K. J. Redox cycling of anthracyclines by cardiac mitochondria. II. Formation of superoxide anion, hydrogen peroxide, and hydroxyl radical. *J. Biol. Chem.* **1986**, *261*, 3068−74.
(69) Upadhyay, K. K.; Bhatt, A. N.; Mishra, A. K.; Dwarakanath, B. S.; Jain, S.; Schatz, C.; Le Meins, J.-F.; Farooque, A.; Chandraiah, G.; Jain, A. K.; Misra, A.; Lecommandoux, S. The intracellular drug delivery and anti tumor activity of doxorubicin loaded poly(γ-benzyl l-glutamate)-b-hyaluronan polymersomes. *Biomaterials* **2010**, *31*, 2882−2892.
(70) Sasidharan, A.; Panchakarla, L. S.; Chandran, P.; Menon, D.; Nair, S.; Rao, C. N. R.; Koyakutty, M. Differential nano-bio interactions and toxicity effects of pristine versus functionalized graphene. *Nanoscale* **2011**, *3*, 2461−2464.
(71) Sasidharan, A.; Panchakarla, L. S.; Sadanandan, A. R.; Ashokan, A.; Chandran, P.; Girish, C. M.; Menon, D.; Nair, S. V.; Rao, C. N. R.; Koyakutty, M. Hemocompatibility and Macrophage Response of Pristine and Functionalized Graphene. *Small* **2012**, *8*, 1251−1263.
(72) Yang, K.; Li, Y.; Tan, X.; Peng, R.; Liu, Z. Behavior and Toxicity of Graphene and Its Functionalized Derivatives in Biological Systems. *Small* **2013**, *9*, 1492−1503.
(73) Matesanz, M.-C.; Vila, M.; Feito, M.-J.; Linares, J.; Gonçalves, G.; Vallet-Regi, M.; Marques, P.-A. A. P.; Portolés, M.-T. The effects of graphene oxide nanosheets localized on F-actin filaments on cell-cycle alterations. *Biomaterials* **2013**, *34*, 1562−1569.
(74) Dietze, E. C.; Caldwell, L. E.; Grupin, S. L.; Mancini, M.; Seewaldt, V. L. Tamoxifen but Not 4-Hydroxytamoxifen Initiates Apoptosis in p53(−) Normal Human Mammary Epithelial Cells by Inducing Mitochondrial Depolarization. *J. Biol. Chem.* **2001**, *276*, 5384−5394.
(75) Wiseman, H.; Halliwell, B. Damage to DNA by reactive oxygen and nitrogen species: role in inflammatory disease and progression to cancer. *Biochem. J.* **1996**, *313*, 17−29.
(76) Matés, J. M.; Sánchez-Jiménez, F. M. Role of reactive oxygen species in apoptosis: implications for cancer therapy. *Int. J. Biochem. Cell Biol.* **2000**, *32*, 157−170.
(77) Tsang, W. P.; Chau, S. P. Y.; Kong, S. K.; Fung, K. P.; Kwok, T. T. Reactive oxygen species mediate doxorubicin induced p53-independent apoptosis. *Life Sci.* **2003**, *73*, 2047−2058.
(78) DiPaola, R. S. To arrest or not to G2-M Cell-cycle arrest: commentary re: AK Tyagi et al., Silibinin strongly synergizes human prostate carcinoma DU145 cells to doxorubicin-induced growth inhibition, G2-M arrest, and apoptosis. *Clin. Cancer Res.* **2002**, *8*, 3311−3314.
(79) Ling, Y. H.; el-Naggar, A. K.; Priebe, W.; Perez-Soler, R. Cell cycle-dependent cytotoxicity, G2/M phase arrest, and disruption of p34cdc2/cyclin B1 activity induced by doxorubicin in synchronized P388 cells. *Mol. Pharmacol.* **1996**, *49*, 832−841.
(80) Potter, A. J.; Gollahon, K. A.; Palanca, B. J.; Harbert, M. J.; Choi, Y. M.; Moskovitz, A. H.; Potter, J. D.; Rabinovitch, P. S. Flow cytometric analysis of the cell cycle phase specificity of DNA damage induced by radiation, hydrogen peroxide and doxorubicin. *Carcinogenesis* **2002**, *23*, 389−401.
(81) Kurz, E. U.; Douglas, P.; Lees-Miller, S. P. Doxorubicin activates ATM-dependent phosphorylation of multiple downstream targets in part through the generation of reactive oxygen species. *J. Biol. Chem.* **2004**, *279*, 53272−81.
(82) Tacar, O.; Pornsak, S.; Dass, C. R. Doxorubicin: an update on anticancer molecular action, toxicity and novel drug delivery systems. *J. Pharm. Pharmacol.* **2013**, *65*, 157−170.

DOI: 10.1021/acsomega.9b03709
ACS Omega 2020, 5, 1656−1668